

1       **Phenotyping metastatic brain tumours applying spectrochemical**  
2                   **analyses: segregation of different cancer types**

3       Danielle Bury<sup>1,\*</sup>, Guy Faust<sup>2</sup>, Maria Paraskevasi<sup>1</sup>, Katherine M. Ashton<sup>3</sup>, Timothy P.  
4                   Dawson<sup>3</sup> and Francis L. Martin<sup>1,\*</sup>

5       <sup>1</sup>*School of Pharmacy and Biomedical Sciences, University of Central Lancashire, Preston*  
6       *PR1 2HE, UK*

7       <sup>2</sup>*Department of Oncology, University Hospitals of Leicester NHS Trust, Leicester,*  
8       *Leicestershire, UK*

9       <sup>3</sup>*Department of Neuropathology, Royal Preston Hospital, Lancashire Teaching Hospitals*  
10       *NHS Trust, Sharoe Green Lane, Preston PR2 9HT, UK*

11

12       Email addresses:

13       [Deb11@doctors.org.uk](mailto:Deb11@doctors.org.uk), [Guy.Faust@uhl-tr.nhs.uk](mailto:Guy.Faust@uhl-tr.nhs.uk), [mparaskevasi@uclan.ac.uk](mailto:mparaskevasi@uclan.ac.uk),  
14       [katherine.ashton@lthtr.nhs.uk](mailto:katherine.ashton@lthtr.nhs.uk), [timothy.dawson@lthtr.nhs.uk](mailto:timothy.dawson@lthtr.nhs.uk), [flmartin@uclan.ac.uk](mailto:flmartin@uclan.ac.uk)

15

16

17       \***Corresponding Authors:** Prof Francis L Martin and Danielle Bury, School of Pharmacy  
18       and Biomedical Sciences, University of Central Lancashire, Preston PR1 2HE, UK;  
19       Telephone: 01772896482; Email: [flmartin@uclan.ac.uk](mailto:flmartin@uclan.ac.uk); [deb11@doctors.org.uk](mailto:deb11@doctors.org.uk)

20

21       The authors declare no competing interests.

22       All authors have contributed equally.

23

24 **Abstract**

25 Metastatic brain tumours represent a significant proportion of tumours identified  
26 intraoperatively. A rapid diagnostic method, circumventing the need for histopathology  
27 studies could prove clinically useful. As many spectroscopic studies have shown ability  
28 to differentiate between different tumour types, this technique was evaluated for use  
29 within metastatic brain tumours. Spectrochemical approaches [Raman and attenuated  
30 total reflection Fourier-transform infrared spectroscopy (ATR-FTIR) spectroscopy]  
31 were applied to determine how readily it could identify the primary site from the  
32 metastatic tumour. Metastases were from primary adenocarcinomas of lung ( $n=7$ ) and  
33 colorectum ( $n=7$ ), and for comparison, metastatic melanoma ( $n=7$ ). The objective was  
34 to determine if Raman or ATR-FTIR spectroscopy could delineate the origin of the  
35 primary tumour. The results demonstrate that there are marked similarities between the  
36 two adenocarcinoma groups and whilst Raman and ATR-FTIR can distinguish the three  
37 groups with limited success, classification accuracy is greatly improved when  
38 combining the adenocarcinoma groups. The use of such techniques in the clinical  
39 setting is more likely to be found intraoperatively, determining the presence of a tumour  
40 and suggesting the tumour class; however, traditional histopathology would still be  
41 needed to identify the primary origin of the tumour.

42 **Keywords:** Attenuated total reflection Fourier-transform infrared (ATR-FTIR)  
43 spectroscopy, classification, linear discrimination analysis (LDA), metastatic brain  
44 tumour, neuro-oncology, Raman spectroscopy

## 45 **Introduction**

46 Metastatic brain tumours are usually the end-point in a persons' battle with cancer,  
47 yet for some may represent the initial diagnosis. The background prevalence of  
48 metastatic brain tumours is difficult to quantify; however, those clinically detectable  
49 outnumber intrinsic tumours by roughly 3 to 1, with the majority of metastases arising  
50 from primary lung tumours (Davis *et. al.* 2012, Huang and Ouyang 2013, Renfrow  
51 and Lesser 2013). In contrast, colorectal tumours comprise 4-8% of metastasis, yet  
52 less than 9% of all cases metastasise to the brain (Sanghvi *et. al.* 2017).

53 Up to 15-25% of brain tumours diagnosed are a metastasis (Bekaert *et. al.* 2017).

54 Whilst 80% of patients have a known primary, for some patients the identification of  
55 metastasis may be the initial presentation of the primary tumour (Bekaert *et. al.*  
56 2017). It is thought that the actual incidence of brain metastases is higher than  
57 reported as some may go undiagnosed. For those who undergo metastectomy for  
58 diagnosis or symptom relief, the tissue, once removed is sent for histopathological  
59 analysis to determine the location of the primary tumour.

60 Currently, diagnosis generally relies upon a mix of haematoxylin and eosin (H&E)  
61 morphological appearances, special tinctorial stains and immunohistochemical (IHC)  
62 tests that enable the pathologist to give either a single or group of organs from which  
63 the primary tumour likely arises. Morphologically these tumours can look remarkably  
64 similar. However, there remains a group of unclassifiable tumours, which are labelled  
65 as 'cancer of unknown primary (CUP)' when histopathology and radiology fails to  
66 determine a primary origin. The challenge can then be to determine the most likely  
67 primary origin in order to guide cancer specific oncological treatment. In an era where

68 cancer treatment is guided more by genetic alterations, such as epidermal growth  
69 factor receptor (EGFR) mutations in lung cancer, to enable personalised treatment, the  
70 need to determine the primary origin to guide genetic testing has never been more  
71 crucial (Kalia 2015).

72 Over recent years many biomarkers have been suggested for identification of disease  
73 and monitoring of disease progression in known cancer patients, such as prostate  
74 specific antigen (PSA) in prostate cancer patients. The difficulty, however, is that not  
75 all patients with prostate cancer will demonstrate a rise in PSA, nor do all patients  
76 with a high PSA have prostate cancer. Whilst it is thought those with prostate cancer  
77 and low PSA represents less than 1% of such patients, as the condition becomes more  
78 prevalent this is likely to increase (Lee *et al.* 2010). Therefore the ability to have a  
79 specific and sensitive marker for tumours is crucial.

80 In recent years, Raman or attenuated total reflection-Fourier transform infrared  
81 (ATR-FTIR) spectroscopy methods have been used to delineate a variety of primary  
82 and metastatic tumours with varying success (Theophilou *et al.* 2015, 2016). Raman  
83 and ATR-FTIR spectroscopy are complimentary techniques; Raman spectroscopy  
84 detects chemical bonds *via* scattering of photons due to bond vibrations, whereas  
85 ATR-FTIR spectroscopy measures energy absorbance after excitation by an infrared  
86 (IR) beam following reflection of the beam *via* an internal element (often diamond or  
87 germanium). Both provide a ‘fingerprint’ of the elements within the examined tissue,  
88 which have been used to differentiate between cancerous and non-cancerous tissue  
89 and biofluids within a variety of studies (Owens *et al.* 2014). Krafft *et al.* (2006)  
90 were able to determine the primary origin from brain metastases of three tumours  
91 using IR spectroscopic imaging with variable success (Krafft *et al.* 2006). They

92 compared normal brain to metastases from lung, colon, breast and renal carcinoma.  
93 Results showed tumour primary site could be delineated; however, there was an  
94 overlap between breast, lung and colorectal carcinomas. A later study by the same  
95 group, again using imaging methods but a broader range of cancers, also  
96 demonstrated similar overlap within the adenocarcinomas (Bergner *et. al.* 2013).  
97 Given the relatively similar morphological appearances and IHC staining results  
98 overlaps, this is not surprising. Gajjar *et. al.* (2012) also demonstrated positive results  
99 in distinguishing different intrinsic brain tumours from normal brain tissue,  
100 demonstrating the ability of Raman and ATR-FTIR spectroscopy to segregate  
101 different tumour types (Gajjar *et. al.* 2012).

102 Outside of the brain, the use of spectroscopy on both tissue and blood components has  
103 shown promise in the detection of many cancers around the body, including skin,  
104 oesophagus, ovary and cervix with varying degrees of success (Krafft *et. al.* 2006,  
105 Gajjar *et. al.* 2012, Lyng *et. al.* 2007, Lui *et. al.* 2012, Kendall *et. al.* 2010, Barr *et. al.*  
106 2011, Mitchell *et. al.* 2014). However, relatively few studies focus on the  
107 differentiation of primary tumour from metastasis. Therefore, within this study, brain  
108 metastasis from lung and colorectal adenocarcinomas have been chosen due to their  
109 similar morphological appearances (see Figure 1), and their ability to often have  
110 challengingly similar IHC staining patterns. Whilst at first glance these tumours may  
111 appear different, it is not possible on morphology alone to determine the definitive  
112 primary location of the tumour and immunohistochemistry is regularly performed.  
113 This limited variability between the two adenocarcinomas will provide a challenge to  
114 determine if Raman and/or ATR-FTIR spectroscopy can detect these differences and  
115 indicate tumour origin. To contrast this, metastatic melanoma was selected since it  
116 provides a marked contrast in both appearances and immunohistochemical staining

117 patterns to the adenocarcinomas (see Figure 1). The initial hypothesis was that the  
118 two adenocarcinoma groups would show similar spectral patterns and therefore would  
119 be difficult to differentiate as compared to the metastatic melanoma group, which  
120 would demonstrate a marked difference. The novelty of this study lies in the  
121 comparison of both Raman and FTIR-ATR within a pre-selected group of metastases,  
122 with the analyses performed on spectral analysis without the need for complex  
123 imaging.

## 124 **Methods**

125 Formalin-fixed paraffin embedded tissue from twenty-one brain metastasis  
126 comprising colorectal adenocarcinoma metastasis ( $n=7$ ), lung adenocarcinomas  
127 metastasis ( $n=7$ ) and metastatic melanomas ( $n=7$ ) were obtained from the Brain  
128 Tumour North West (BTNW) research tissue bank (RTB – ethics NRES14/EE/1270).  
129 Sections (10- $\mu$ m-thick) were placed onto glass slides covered with aluminium foil.  
130 Foil-covered slides have been previously demonstrated to be as effective as more  
131 expensive substrates significantly reducing the costs of this process (Cui *et al.* 2016;  
132 Paraskevaidi *et al.* 2018). These were de-waxed prior to spectral acquisition by  
133 leaving overnight in fresh xylene. They were then washed in fresh xylene for 5 min.  
134 Following this, they were immersed in fresh ethanol at 100% twice and then 70%  
135 ethanol once, for 5 min each, and then allowed to air dry prior to spectral acquisition.  
136 H&E-stained slides were viewed to delineate the tumour to be examined, to reduce  
137 contamination of spectra from background brain tissue.

138

139 ***Raman spectroscopy***

140 A Renishaw InVia Raman spectrometer was used to collect 25 spectra per section  
141 using a 785 nm laser at 1200 g mm<sup>-1</sup> grating with an acquisition time of 30 seconds  
142 for each sample. This was over a spectral range of 400-1600 cm<sup>-1</sup>. A 50× objective  
143 with numerical aperture of 0.85 was used to focus the laser beam. The spectral sites  
144 were selected at random moving over the tissue.

145 ***Attenuated total reflection Fourier-transform infrared (ATR-FTIR) spectroscopy***

146 ATR-FTIR spectra were collected using a Bruker Tensor 27 Fourier transform  
147 infrared spectrometer with Helios attenuated total reflection attachment containing a  
148 diamond crystal internal reflective element and a 45° incidence angle of infrared  
149 beam. A new background spectrum was collected prior to each new sample, following  
150 cleaning of the crystal with distilled water. For each case 32 scans with 8 cm<sup>-1</sup>  
151 spectral resolution were taken at 10 randomly selected points. The sampling aperture  
152 was 250 μm × 250 μm and the mirror velocity was 2.2 Hz.

153 ***Computational analyses***

154 Computational analyses, including principal component analysis (PCA) with linear  
155 discriminant analysis (LDA) and linear discriminant classifier (LDC) was then  
156 performed within a MATLAB (Mathworks, Natick, USA) environment, using the  
157 IRootlab toolkit as a user interface (Martin *et al.* 2010, Trevisan *et al.* 2013,  
158 Paraskevaidi *et al.* 2017). For classification spectra were pre-processed by cutting to  
159 the region of interest (Raman = 500-1800 cm<sup>-1</sup>; ATR-FTIR = 900-1800 cm<sup>-1</sup>),  
160 followed by polynomial baseline correction and vector normalisation. Spectra were

161 then interrogated *via* PCA-LDA to generate scores plots and cluster vectors to  
162 determine points of variation between the spectra; PCA-LDC was then applied to  
163 calculate the classification accuracy as compared to the histopathological result. The  
164 top 6 spectral differences between the adenocarcinoma and melanoma groups were  
165 also determined.

## 166 **Results**

167 Analysis of the spectra has shown similar results for both Raman and ATR-FTIR  
168 spectroscopy. They demonstrate similar spectral appearances for both  
169 adenocarcinoma groups, with significant differences seen to the spectra of the  
170 melanoma. This can be seen primarily within both the pre-processed spectra [see  
171 Figure 2]. The lines for both adenocarcinoma groups show little variance, with the  
172 melanoma line clearly being separated at several points.

173 PCA-LDA was carried out to determine the principal components and thus the factors  
174 that account for most variance between the three groups in order to classify them. It  
175 was demonstrated that the groups show a degree of overlap (see Figure 3), which is  
176 greatest between the two adenocarcinoma groups. The points within the clusters show  
177 little difference within the adenocarcinoma groups, though the melanoma group is  
178 clearly separated, with little overlap of the confidence bubbles. From this, cluster  
179 vectors were used to visualise the differences between the three groups. It can be seen  
180 (Figure 4) that the two adenocarcinoma groups are similar with small areas of  
181 variance (Figure 4 D/d) as the lines are almost superimposed upon each other.  
182 However, the melanoma groups show a marked difference, with much greater  
183 separation of the two lines. This is particularly demonstrated within panel (D/d) where

184 melanoma is taken as the baseline. This shows how similar adenocarcinomas are  
185 despite their different primary locations.

186 A PCA-LDC, giving the classification accuracy for each group as compared to the  
187 final histological diagnosis, was then performed (Figure 5). This was run for three  
188 separate groups and then two (combining the two adenocarcinoma groups) groups to  
189 show the difficulty in separating the adenocarcinomas. When using three groups for  
190 Raman, the classification accuracy is 69% for colorectal adenocarcinoma, 69% for  
191 lung adenocarcinoma and 72% for melanoma. Using ATR-FTIR spectroscopy this is  
192 60% for colorectal adenocarcinoma, 59% for lung adenocarcinoma and 47% for  
193 melanoma. If the two adenocarcinoma groups are combined, classification accuracy  
194 markedly increases. With Raman spectroscopy this improves to 85% for  
195 adenocarcinoma and 75.4% for melanoma, and with ATR-FTIR spectroscopy 96%  
196 for adenocarcinoma and 72% for melanoma. This is, however, still below that found  
197 with traditional histopathology.

198 Following this, a one-way Anova was performed for the three groups to assess if the  
199 differences seen between the spectra were significant. A student's *t*-test was  
200 performed on the merged 2 groups to assess significance due to the small numbers  
201 involved (Figure 6). This was performed on the PCA-LDA results using all spectra  
202 for each case. For the three Raman spectroscopy groups this was  $P=0.0016$  at 95%  
203 confidence interval and for ATR-FTIR spectroscopy this was not significant ( $P=0.08$ )  
204 [see Supplementary information (SI) Table S1]. For two groups, this was again  
205 significant at  $<0.0001$  for Raman and ATR-FTIR, with a 95% confidence interval (see  
206 SI Table S2).

207 The statistical significance between each group was also calculated using a one-way  
208 Anova (see SI Table S1). This highlights the statistically significant differences found  
209 between adenocarcinoma and melanoma. There is no statistical difference between  
210 the two adenocarcinoma groups on either Raman or ATR-FTIR spectroscopy.

211 To conclude, the significant differences were calculated (see Figure 7) and tentative  
212 distinguishing wavenumbers assigned to those differences (Table 1). This was done to  
213 examine the points at which the tumours vary and to see which areas accounted for  
214 the variation. Within both Raman and ATR-FTIR spectroscopy the main variances  
215 were found within CH<sub>2</sub> bond deformation and methylene twisting regions. Changes  
216 within these regions have previously been reported within carcinogenic samples  
217 (Movasaghi, Rehman and Rehman 2007, 2008) of varying types. Therefore, perhaps  
218 these regions are tied to carcinogenesis and not the particular tumour type with  
219 variations seen depending on the tumour.

## 220 **Discussion**

221 Both spectroscopic methods have been shown to be able to classify the different  
222 tumours by type (*i.e.*, adenocarcinoma vs. melanoma), providing similar results.  
223 However, accuracy is greatly diminished if it is used to classify the primary origin of  
224 the tumour type, specifically determining if the adenocarcinoma arose within the lung  
225 or colon. Minor differences are seen between the spectra of these two tumours (see  
226 Figure 2); however, these differences are not statistically significant. This would,  
227 therefore, limit any clinical use, as it would not be able to provide as much  
228 information as traditional histopathology with H&E and IHC. It may be that such new  
229 tools may aid the clinician in determining tumour type intra-operatively, *i.e.* that the  
230 tumour is a metastasis and not a primary brain tumour, but formal histopathology with

231 IHC would still be required for primary tissue origin identification. This, however, is  
232 also of interest given the marked spectral similarities between adenocarcinomas of  
233 different primary origins (Figures 2 and 4). Within this study, confounding factors,  
234 such as the number or location of the brain metastasis, nor patient factors have been  
235 used to contribute to the accuracy of the results. As this was a comparison to  
236 conventional histopathology, these factors would not impact upon microscopy or  
237 immunohistochemistry, therefore it was felt not appropriate to be added into the  
238 diagnostic algorithm.

239 When evaluating the potential value of spectroscopy as a possible intraoperative tool  
240 its ability to determine cancer versus no cancer and suggest a tumour type would be  
241 required. To provide further information to that provided by intraoperative  
242 neuropathology, spectroscopy would need to differentiate the primary tumour origin  
243 for a metastasis. However, as can be seen, both Raman and ATR-FTIR spectroscopy  
244 are able to detect differences between the two tumour types, but not specify the  
245 primary tissue origin accurately enough for treatment decisions. As the technique  
246 develops, it may replace frozen section, often performed intraoperatively to determine  
247 if a tumour is primary, *i.e.*, has arisen within the brain, or is a metastasis to guide the  
248 surgeon in relation to the extent of the resection he may perform, as has been  
249 suggested previously (Ji *et. al.* 2013, Ji *et. al.* 2015, Hollon *et. al.* 2016). At which  
250 point, acknowledgement of a metastasis (from a primary tumour) would be the level  
251 required with histopathology completing the primary tumour origin determination as  
252 currently occurs. This would provide a potentially useful area for the technology to  
253 exploit as frozen section work can be challenging and potentially an area for error to  
254 be removed by use of spectroscopy. However, comparative work to normal brain

255 tissue and primary tumours would be required to ensure the technique is able to  
256 differentiate all potential results.

257

## 258 **Conclusion**

259

260 This study has highlighted both forms of spectroscopy are able to differentiate  
261 different tumour types such as melanoma versus adenocarcinoma. However, it is not  
262 able to differentiate tumour types to determine primary tissue origin of a metastasis in  
263 its current form.

264 As the technique develops, it may eventually be able to provide additional  
265 information to support the initial histopathological diagnosis, which may in the future  
266 provide treatment related or prognostic information once the spectra are fully  
267 understood in the years to come.

268 **Conflicts of Interest** The authors declare no conflicts of interest.

## 269 **Acknowledgements**

270 The authors would like to acknowledge the support from Rosemere Cancer  
271 Foundation and the Brain Tumour North West RTB and the Sidney Driscoll  
272 Neuroscience Foundation for their support.

273 Part of this work has been previously published as an abstract at the 2017  
274 American Society of Clinical Oncology Meeting. J Clin Oncol 35, 2017 (suppl:  
275 abstr e13551).

276

277 **References**

278

- 279 Barr, H., C. Kendall, J. Hutchings, F. Bazant-Hegemark, N. Shepherd and N. Stone.  
280 2011. Rapid endoscopic identification and destruction of degenerating Barrett's  
281 mucosal neoplasia. *Surgeon*, 9:119-123.
- 282 Bekaert, L., E. Emery, G. Levallet, and E. Lechapt-Zalcman. 2017. Histopathologic  
283 diagnosis of brain metastases: current trends in management and future  
284 considerations. *Brain Tumour Pathology*, 34:8-19.
- 285 Bergner, N., F. M. Romeike, R. Reichart, R. Kalff, C. Krafft, and J. Popp. 2013.  
286 Tumor margin identification and prediction of the primary tumour from brain  
287 metastases using FTIR imaging and support vector machines. *Analyst*, 138:3983-  
288 3990.
- 289 Cui, L., H. J. Butler, P. L. Martin-Hirsch, and F. L. Martin. 2016. Aluminium foil  
290 as a potential substrate for ATR-FTIR, transflection FTIR or Raman  
291 spectrochemical analysis of biological samples. *Analytical Methods*, 8:481-487.
- 292 Davis, F. G., T. A. Dolecek, B. J. McCarthy, and J. L. Villano. 2012. Toward  
293 determining the lifetime occurrence of metastatic brain tumours estimated from  
294 2007 United States cancer incidence data. *Neuro-Oncology*, 14:1171-1177.
- 295 Gajjar, K., L .D. Heppenstall, W. Pang, K. M. Ashton, J. Trevisan, I. I. Patel, V.  
296 Llabjani, H. F. Stringfellow, P. L. Martin-Hirsch, T. Dawson, and F. L. Martin.  
297 2012. Diagnostic segregation of human brain tumours using Fourier-transform  
298 infrared and/or Raman spectroscopy coupled with discriminant analysis. *Analytical*  
299 *Methods*, 5:89-102.
- 300 Hollon, T., S. Lewis, C. W. Freudiger, X. S. Xie, and D. A. Orringer. 2016.  
301 Improving the accuracy of brain tumor surgery via Raman-based technology.  
302 *Neurosurgical Focus*, 40:3-19.

303 Huang, Q., and X. Ouyang. 2013. Predictive biochemical-markers for the  
304 development of brain metastases from lung cancer: clinical evidence and future  
305 directions. *Cancer Epidemiology*, 37:703-707.

306 Ji, M., D. A. Orringer, C. W. Freudiger, S. Ramkissoon, X. Liu, D. Lau, A. J.  
307 Golby, I. Norton, M. Hayashi, N. Y. R. Agar, G. S. Young, C. Spino, S. Santagata,  
308 S. Camelo-Piragua, K. L. Ligon, O. Sagher, and X. S. Xie. 2013. Rapid, label-free  
309 detection of brain tumours with stimulated Raman scattering microscopy. *Science*  
310 *Translational Medicine*, 5:201-224.

311 Ji, M., S. Lewis, S. Camelo-Piragua, S. H. Ramkissoon, M. Snuderl, S. Venneti, A.  
312 Fisher-Hubbard, M. Garrard, D. Fu, A. C. Wang, J. A. Heth, C. O. Maher, N. Sanai,  
313 T. D. Johnson, C. W. Freudiger, O. Sagher, X. S. Xie, and D. A. Orringer. 2015.  
314 Detection of human brain tumor infiltration with quantitative stimulated Raman  
315 scattering microscopy. *Science Translational Medicine*, 7:309-337.

316 Kalia, M. 2015 Biomarkers for personalized oncology: recent advances and future  
317 challenges. *Metabolism Clinical and Experimental*, 64:S16-21.

318 Kendall, C., J. Day, J. Hutchings, B. Smith, N. Shepherd, H. Barr, and N. Stone.  
319 2010. Evaluation of Raman probe for oesophageal cancer diagnostics. *Analyst*,  
320 135:3038-3041.

321 Krafft, C., L. Shapoval, S. B. Sobottka, K. D. Geiger, G. Schackert, and R. Salzer.  
322 2006. Identification of primary tumours of brain metastases by SIMCA  
323 classification of IR spectroscopic images. *Biochimica et Biophysica Acta*,  
324 1758:883-891.

325 Lee, D. K., J. H. Park, J. H. Kim, S. J. Lee, M. K. Jo, M. C. Gil, K. H. Song, and J.  
326 W. Park. 2010. Progression of Prostate Cancer Despite an Extremely Low Serum  
327 Level of Prostate-Specific Antigen. *Korean Journal of Urology*, 51:358-361.

328 Lui, H., J. Zhao, D. McLean, and H. Zeng. 2012. Real-time Raman Spectroscopy  
329 for in vivo skin cancer diagnosis. *Cancer Resources*, 72:2491-2527.

330 Lyng, F. M., E. O'Faolain, J. Conroy, A. Meade, P. Knief, B. Duffy, M. B. Hunter,  
331 J. M. Byrne, P. Kelehan, and H. J. Byrne. 2007. Vibrational spectroscopy for  
332 cervical cancer pathology, from biochemical analysis to diagnostic tool,  
333 *Experimental and Molecular Pathology*, 82:121-129.

334 Martin, F. L., J. G. Kelly, V. Llabjani, P. L. Martin-Hirsch, I. I. Patel, J. Trevisan,  
335 N. J. Fullwood, and M. J. Walsh. 2010. Distinguishing cell types or populations  
336 based on the computational analysis of their infrared spectra. *Nature Protocols*, 5:  
337 1748-1760.

338 Mitchell, A. L., K. B. Gajjar, G. Theophilou, F. L. Martin, and P. L. Martin-Hirsch.  
339 2014. Vibrational spectroscopy of biofluids for disease screening or diagnosis:  
340 translation from the laboratory to a clinical setting. *Journal of Biophotonics*, 7:153-  
341 165.

342 Movasaghi, Z., S. Rehman, and I. Rehman. 2007. Raman Spectroscopy of  
343 Biological Tissues. *Applied Spectroscopy Reviews*, 42:493-541.

344 Movasaghi, Z., S. Rehman, and I. Rehman. 2008. Fourier Transform Infrared  
345 (FTIR) Spectroscopy of Biological Tissues. *Applied Spectroscopy Reviews*,  
346 43:134-179.

347 Owens, G. L., K. Gajjar, J. Trevisan, S. W. Fogarty, S. E. Taylor, B. Da Gama-  
348 Rose, P. L. Martin-Hirsch, and F. L. Martin. 2014. Vibrational biospectroscopy  
349 coupled with multivariate analysis extracts potentially diagnostic features in blood  
350 plasma/serum of ovarian cancer patients. *Journal of Biophotonics*, 7:200-209.

351 Paraskevaidi, M., C. L. M. Morais, K. M. G. Lima, J. S. Snowden, J. A. Saxon, A.  
352 M. T. Richardson, M. Jones, D. M. A. Mann, D. Allsop, P. L. Martin-Hirsch, and

353 F. L. Martin. Differential diagnosis of Alzheimer's disease using spectrochemical  
354 analysis of blood. *Proceedings of the National Academy of Sciences USA*, 114:  
355 E7929-E7938.

356 Paraskevaidi, M., C. L. M. Morais, O. Raglan, K. M. G. Lima, E. Paraskevaidis, P.  
357 L. Martin-Hirsch, M. Kyrgiou, and F. L. Martin. 2018. *Journal of Biophotonics*,  
358 doi: 10.1002/jbio.201700372.

359 Renfrow, J. J., and G. J. Lesser. 2013. Molecular subtyping of brain metastases and  
360 implications for therapy. *Current Treatment Options in Oncology*, 14:514-527.

361 Sanghvi, S. M., J. W. Lischalk, L. Cai, S. Collins, M. Nair, B. Collins, and K.  
362 Unger. 2017. Clinical outcomes of gastrointestinal brain metastases treated with  
363 radiotherapy. *Radiation Oncology*, 12:43-51.

364 Theophilou, G., M. Paraskevaidi, K. M. Lima, M. Kyrgiou, P. L. Martin-Hirsch,  
365 and F. L. Martin. 2015. Extracting biomarkers of commitment to cancer  
366 development: potential role of vibrational spectroscopy in systems biology. *Expert*  
367 *Review of Molecular Diagnostics*, 15:693-713.

368 Theophilou, G., K. M. Lima, P. L. Martin-Hirsch, H. F. Stringfellow, and F. L.  
369 Martin. 2016. ATR-FTIR spectroscopy coupled with chemometric analysis  
370 discriminates normal, borderline and malignant ovarian tissue: classifying subtypes  
371 of human cancer. *Analyst*, 141:585-594.

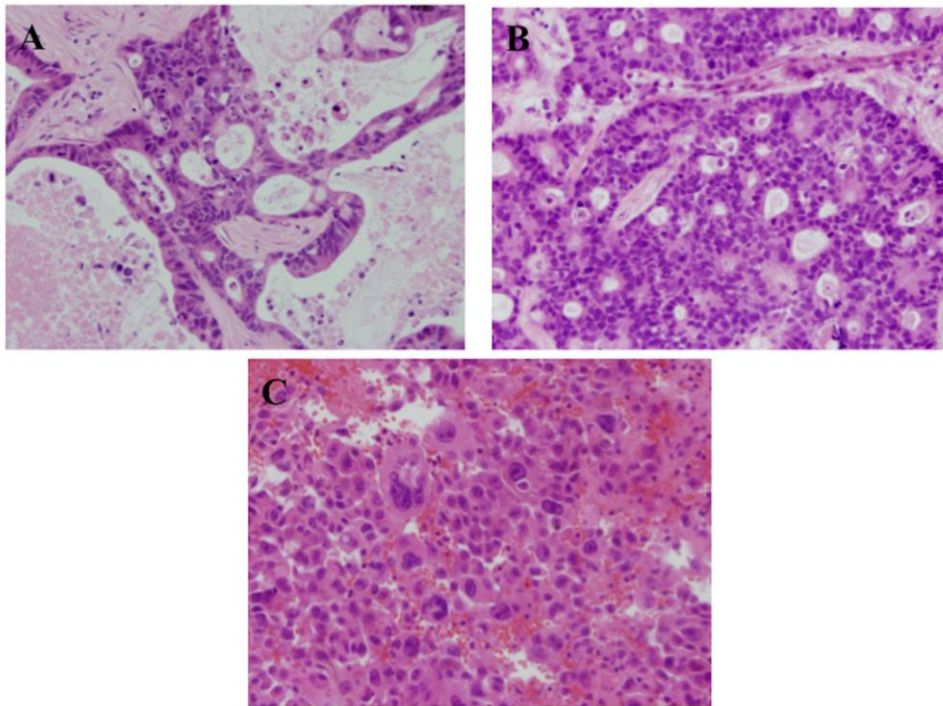
372 Trevisan, J., P. P. Angelov, A. D. Scott, P. L. Carmichael, and F. L. Martin. 2013.  
373 IRRootLab: a free and open-source MATLAB toolbox for vibrational  
374 biospectroscopy data analysis. *Bioinformatics*, 29:1095-1097.

375

376

377 **Table 1** The tentative assignments of significant points of difference for Raman and  
 378 attenuated total reflection-Fourier transform infrared (ATR-FTIR) spectroscopy,  
 379 using adenocarcinoma *vs.* melanoma (Movasaghi, Rehman and Rehman 2007, 2008).

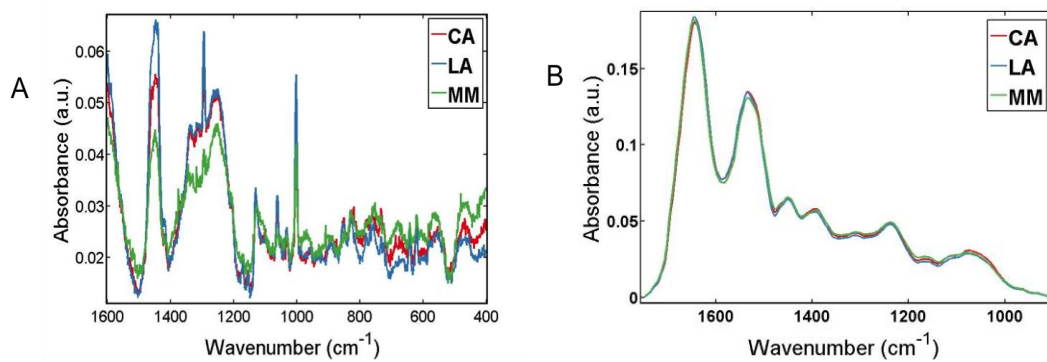
Method	Wavenumber (cm <sup>-1</sup> )	Tentative assignment
Raman	1310	CH <sub>3</sub> /CH <sub>2</sub> twisting or bending mode of lipid/collagen CH <sub>3</sub> /CH <sub>2</sub> twisting, wagging &/or bending mode of collagens & lipids
	1297	CH <sub>2</sub> deformation/Palmitic acid, acyl chains, fatty acids
	1296	CH <sub>2</sub> deformation
	1295	Methylene twisting /CH <sub>2</sub> deformation
	1294	Methylene twisting
	1293	Cytosine/ Methylene twisting
ATR-FTIR	1720	C=O
	1578	Ring C-C stretch of phenyl
	1481	Amide II
	1477	CH <sub>2</sub> bending of methylene chains in lipids /Polyethylene methylene of deformation modes
	1474	CH <sub>2</sub> bending of methylene chains in lipids /Polyethylene methylene of deformation modes
	1470	CH <sub>2</sub> bending of methylene chains in lipids



380

381 **Figure 1** Representative photomicrographs of the microscopic appearance of brain  
382 metastasis from different primary tumour sites. (A) is a metastasis from a colorectal  
383 adenocarcinoma (H&E  $\times 200$  objective); (B) is a metastasis from a lung  
384 adenocarcinoma (H&E  $\times 200$  objective); and, (C) is a metastasis from a malignant  
385 melanoma (H&E  $\times 200$  objective).

386

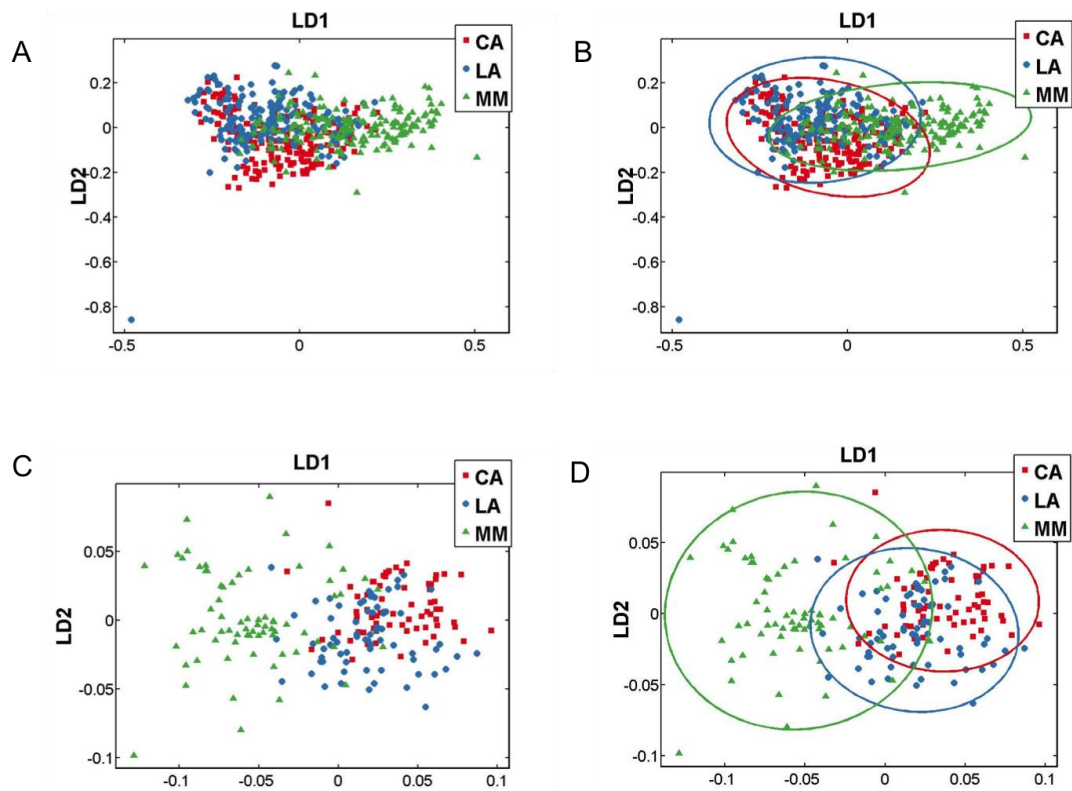


387

388 **Figure 2** A graph demonstrating the mean pre-processed spectra from each tumour  
 389 group using: (A) Raman spectroscopy (cut to the region of interest, polynomial  
 390 baseline correction and vector normalisation); and, (B) ATR-FTIR spectroscopy (cut  
 391 to the region of interest, rubberband baseline correction and vector normalisation).  
 392 (KEY: CA=COLORECTAL ADENOCARCINOMA, LA=LUNG ADENOCARCINOMA,  
 393 MM=MELANOMA).

394

395



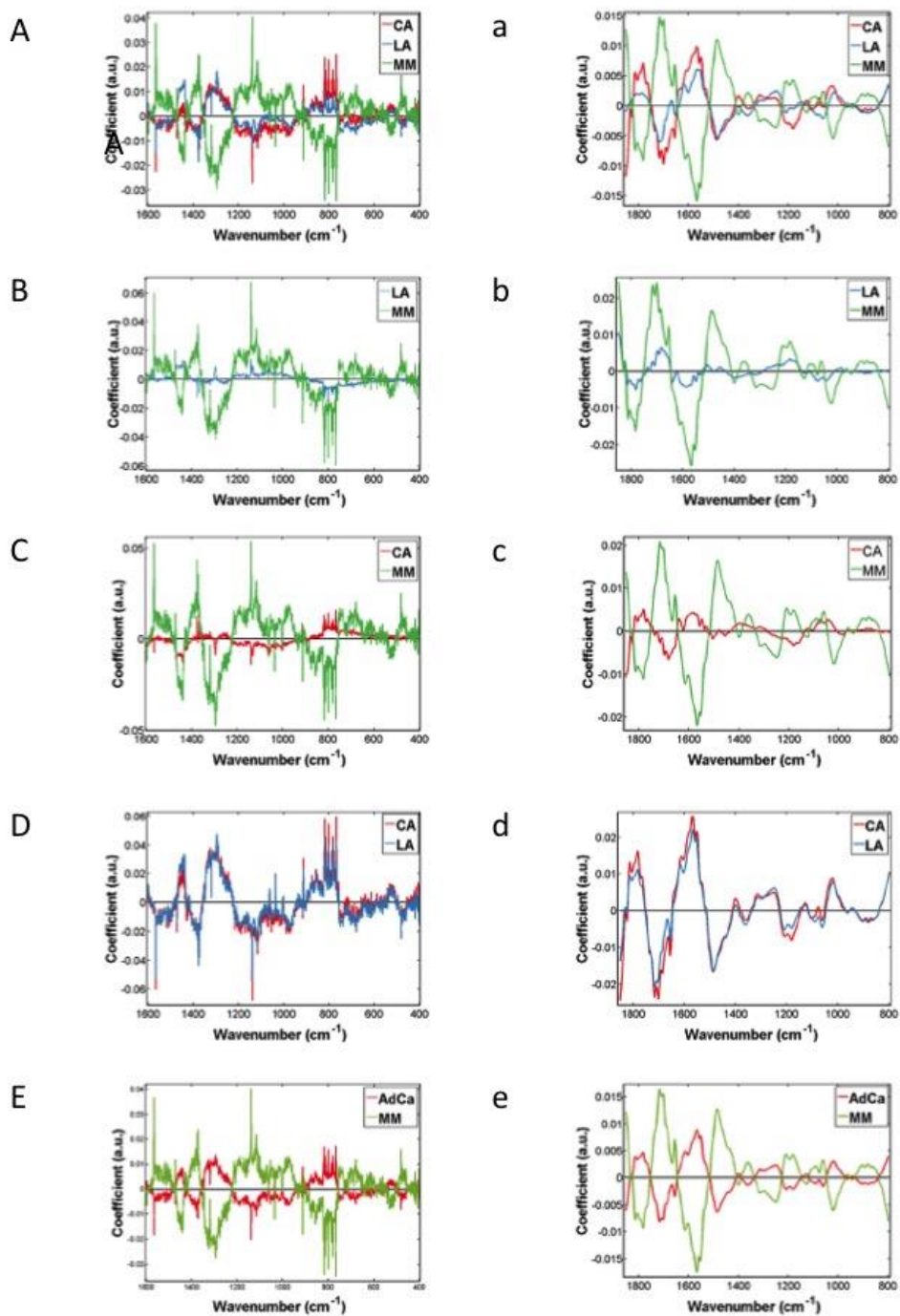
396

397

398 **Figure 3** A graph demonstrating the PCA-LDA results for Raman and ATR-FTIR  
 399 spectroscopy. The left side demonstrates the Raman spectroscopy results firstly  
 400 without (A) and secondly with (B) 95% confidence intervals. This is then mirrored on  
 401 the right for ATR-FTIR spectroscopy, without (C) and with (D) 95% confidence  
 402 intervals. (KEY: CA – COLORECTAL ADENOCARCINOMA, LA – LUNG  
 403 ADENOCARCINOMA, MM – MALIGNANT MELANOMA)

404

405

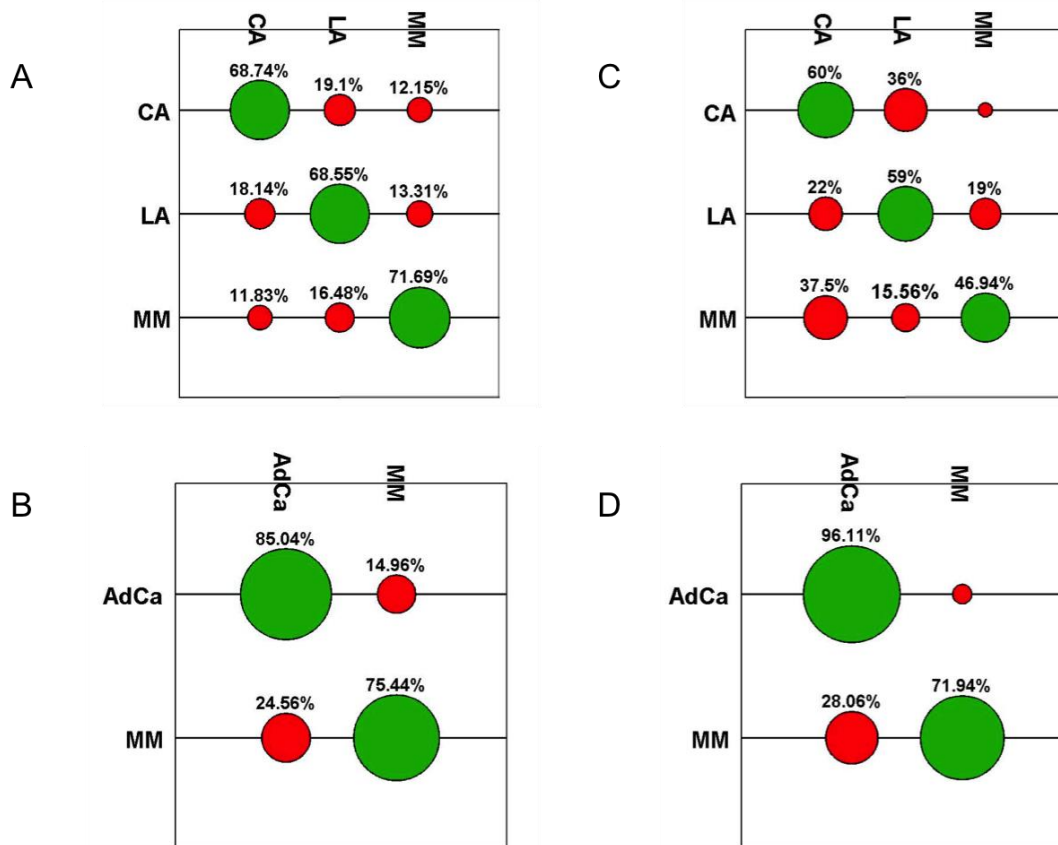


406

407

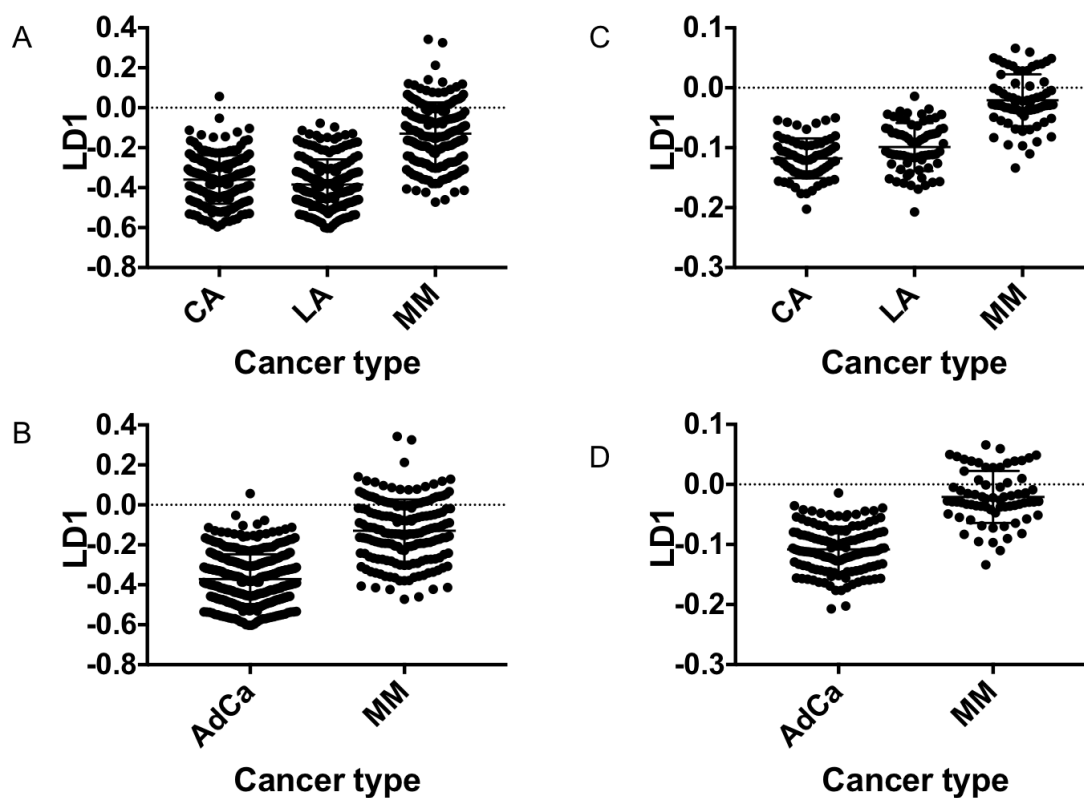
408 **Figure 4** These graphs show the cluster vectors for Raman and ATR-FTIR  
 409 spectroscopy. The upper case displays the Raman spectroscopy results, starting  
 410 with (A/a) all the groups, (B/b) CA is taken as the baseline, (C/c) LA taken as  
 411 the baseline, (D/d) MM taken as baseline and (E/e) compares adenocarcinoma

412 vs. MM. This is mirrored on the right, with lower case letters for ATR-FTIR  
413 spectroscopy. (KEY: CA – COLORECTAL ADENOCARCINOMA, LA – LUNG  
414 ADENOCARCINOMA, MM – MALIGNANT MELANOMA, AdCA –  
415 ADENOCARCINOMA).  
416



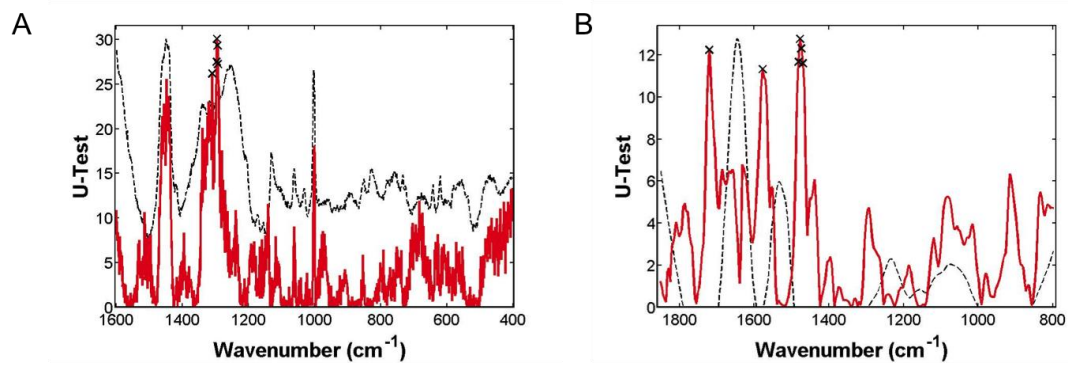
417

418 **Figure 5** The confusion matrices display the percentage of the results assigned to the  
 419 correct group (green) or another group (red). The Raman results are shown on the left  
 420 with (A) displaying each of the three cancer groups separately, and (B) compares  
 421 adenocarcinoma to MM. On the right are the ATR-FTIR spectroscopy results; (C)  
 422 displays each of the three cancer groups separately and (D) again compares  
 423 adenocarcinoma to MM. (KEY: CA – COLORECTAL ADENOCARCINOMA, LA –  
 424 LUNG ADENOCARCINOMA, MM – MALIGNANT MELANOMA, AdCa –  
 425 ADENOCARCINOMA).



426

427 **Figure 6** These graphs represent the results of both a one-way Anova and student's *t*-  
 428 test scores plot for Raman and ATR-FTIR spectroscopy. (A) shows the one-way  
 429 Anova for Raman with all three tumour groups, (B) the student's *t*-test for Raman  
 430 spectroscopy with adenocarcinoma and MM. This is mirrored for ATR-FTIR  
 431 spectroscopy with (C) showing the one-way Anova for ATR-FTIR spectroscopy with  
 432 all three tumour groups and (D) the student's *t*-test for ATR-FTIR spectroscopy with  
 433 adenocarcinoma and MM. (KEY: CA – COLORECTAL ADENOCARCINOMA, LA –  
 434 LUNG ADENOCARCINOMA, MM – MALIGNANT MELANOMA).



435

436 **Figure 7** The significant wavenumber differences between the adenocarcinoma

437 groups and melanoma. (A): Raman spectroscopy, (B): ATR-FTIR spectroscopy